Full Multiple Scattering and Crystal Field Multiplet Calculations Performed on the Spin Transition $Fe^{II}(phen)_2(NCS)_2$ Complex at the Iron K and $L_{2,3}$ X-ray Absorption Edges

V. Briois,*,† Ch. Cartier dit Moulin,† Ph. Sainctavit,†,‡ Ch. Brouder,†,§ and A.-M. Flank†

Contribution from LURE, CNRS-CEA-MEN UMR 130, Bat. 209D, UPS, 91405 Orsay Cedex, and LMCP, CNRS-URA 9, Universités Paris 6 et 7, 4 place Jussieu, 75252 Paris Cedex 05, France, and LPS, CNRS, Université de Nancy I, 54506 Vandœuvre-lès-Nancy Cedex, France

Received May 16, 1994[⊗]

Abstract: The pseudooctahedral $Fe^{II}(phen)_2(NCS)_2$ (where phen = 1,10-phenanthroline) complex is well-known for its changing spin state under external perturbations like temperature. In this paper, a detailed X-ray absorption study of the thermally induced spin transition at the iron K and $L_{2,3}$ edges is presented. The XANES features at both edges are extremely sensitive to the spin state. But insofar as the spin transition is associated simultaneously with a change in the magnetic state, $S = 2 \rightleftharpoons S = 0$, and a modification of the atomic arrangement, the attribution of strong changes in XANES spectra is not obvious. In order to sort out the nature of these modifications, we have performed calculations of the X-ray absorption cross sections at both edges. In the framework of the multiple scattering theory, we have calculated the iron K edge spectra of both spin states, and by using the multiplet picture in the intermediate crystal field framework, we have simulated the iron $L_{2,3}$ edge spectra of both spin states. We show that the main XANES changes at the K edge are related to the structural modifications around the iron, whereas those at the $L_{2,3}$ edges are due to the change of the occupancy of the 3d levels split by the pseudooctahedral crystal field. Furthermore, we show that multiplet calculations give precise information about the ground state of iron(II) in O_h symmetry. We have determined the $10Dq$ crystal field strengths in both spin states and compared them with those determined by optical spectroscopy. In the low-spin state, both visible and X-ray spectroscopies give comparable values, but we observe a large discrepancy in the high-spin state. Analyzing the *LS* terms of the ground state and their energies for both spin states, we discuss, in the case of the $3d^6$ iron ion, the effect of the $10Dq$ values introduced in the multiplet calculations in reproducing experimental spectra and explaining the discrepancy between $10Dq$ values extracted from the two spectroscopies for the high-spin state.

Introduction

X-ray absorption spectroscopy has the peculiar property of being sensitive to both structural and electronic changes in a selected target atom. Therefore, this technique is particularly adapted to the study of physical phenomena involving modifications like spin crossover. In previous papers, we have reported X-ray absorption spectroscopy studies of the iron K[1,2] and $L_{2,3}$[3] edges of the $Fe^{II}(phen)_2(NCS)_2$ (where phen = 1,10-phenanthroline) complex above and below the critical temperature of spin interconversion (T_c = 176 K). We have shown that the XANES parts of the X-ray absorption spectra—the fine structure near the edge—at the three edges are strongly modified during this spin transition. The spin crossover, $S = 2$ (paramagnetic state) $\rightleftharpoons S = 0$ (diamagnetic state), in this molecular $Fe^{II}(phen)_2(NCS)_2$ complex has been extensively studied over the past 30 years by various techniques: magnetic susceptibility measurements,[4−7] vibrational and electronic spectroscopies,[4,7−9] Mössbauer[6,7,9] and calorimetric measurements,[6,10,11] X-ray diffraction,[6,12] and X-ray absorption spectroscopy.[1−3] All these studies showed that the spin crossover is associated with changes in both structural and electronic states. On the one hand, EXAFS analysis, performed at the iron K edge of the same sample, reveals a contraction (ΔR = 0.24 Å) of the first coordination shell around iron upon transition from the high- to low-spin state.[1] This contraction of the structure has been confirmed by X-ray diffraction measurements on a different kind of preparation of the $Fe^{II}(phen)_2(NCS)_2$ sample.[12] On the other hand, electronic spectra analysis, in the region characteristic of d−d transitions, reveals an increase in the ligand field parameter $\Delta 10Dq \approx 4400$ cm^{-1} (0.55 eV) during the spin transition of the $Fe^{II}(phen)_2(NCS)_2$ complex.[7]

† LURE, Université Paris-Sud, Orsay Cedex.
‡ LMCP, Université Paris, Paris Cedex.
§ Université de Nancy I.
⊗ Abstract published in *Advance ACS Abstracts*, December 15, 1994.

(1) Cartier, C.; Thuery, P.; Verdaguer, M.; Zarembowitch, J.; Michalowicz, A. *J. Phys.* **1986**, C8, *47*, 563.
(2) Cartier dit Moulin, C.; Sainctavit, P.; Briois, V. In *Proceedings of the Seventh International Conference on X-Ray Absorption Fine Structure*, Kobe, Japan, 1992; *Jpn. J. Appl. Phys.* **1993**, *32*, 38.
(3) Cartier dit Moulin, C.; Rudolf, P.; Flank, A.-M.; Chen, C. T. *J. Phys. Chem.* **1992**, *96*, 6196.
(4) König, E.; Madeja, K. *Chem. Commun.* **1966**, *3*, 61.
(5) Müller, E. W.; Spiering, H.; Gütlich, P. *Chem. Phys. Lett.* **1982**, *93*, 567.
(6) Ganguli, P.; Gütlich, P.; Müller, E. W. W.; Irler, W. *J. Chem. Soc., Dalton Trans.* **1981**, 441.
(7) König, E.; Madeja, K. *Inorg. Chem.* **1967**, *6*, 67.
(8) Baker, W. A., Jr.; Long, G. J. *Chem. Commun.* **1965**, *15*, 368.
(9) Savage, S.; Jia-Long, Z.; Maddock, A. *J. Chem. Soc., Dalton Trans.* **1985**, 991.
(10) Gütlich, P. *Struct. Bonding (Berlin)* **1981**, *44*, 83.
(11) Sorai, M.; Seki, S. *J. Phys. Chem. Solids* **1974**, *35*, 555.
(12) Gallois, B.; Real, J.-A.; Hauw, C.; Zarembowitch, J. *Inorg. Chem.* **1990**, *29*, 1152.

0002-7863/95/1517-1019$09.00/0

Insofar as both structural and electronic changes are intimately correlated (for $Fe^{II}(phen)_2(NCS)_2$, an increase in the ligand field strength leads to a decrease in the volume of the coordination shell and *vice versa*), the origin of the strong XANES modifications observed at the iron K and L edges is not obvious. Therefore, to sort out the nature of these modifications, we performed calculations of X-ray absorption K and $L_{2,3}$ spectra for the two spin isomers of the $Fe^{II}(phen)_2(NCS)_2$ complex. Because of the high number of studies of the spin transition of this $Fe^{II}(phen)_2(NCS)_2$ complex,[4-12] we had enough structural and electronic information to guide our calculations. Furthermore, the choice of this compound is justified in this way: (i) it presents a complete spin transition, which is very useful in performing significant calculations, and (ii) the iron oxidation degree is (II). It is known that the structural and electronic changes involved in the spin transition of two electrons from the antibonding 3d orbitals of symmetry e_g to the orbitals of t_{2g} symmetry in a Fe(II) complex ($3d^6$) in an octahedral environment are more important than in the Fe(III) or Co(II) complexes ($3d^5$). Indeed, there is a great stabilization of the low-spin form because the t_{2g} levels are totally occupied. Therefore, this complex is a very good model with which to check the capability of the X-ray absorption spectroscopy to investigate such systems and principally to test the validity of the two usual theoretical approaches that describe the K and $L_{2,3}$ edges.

The calculations have been performed in the framework of the multiple scattering theory for the K absorption edge and using a crystal field formalism for the $L_{2,3}$ absorption edges. Although the goal of both theories is the same, to calculate the square of the electric dipole matrix element $\langle\psi_{ex}|\hat{O}|\psi_{gr}\rangle$, where ψ_{ex} (respectively ψ_{gr}) is the excited state wave function (respectively the ground state) and $\hat{O}$ is the electric dipole transition operator, both frameworks do not describe the same kind of states. Multiple scattering theory is a one-electron theory derived from KKR band structure calculations. Since it applies in real space, it is particularly suited to X-ray absorption spectroscopy, which has long been known as a short range process. Multiple scattering can be applied to K edges because they correspond to transitions from the 1s core level to p states. For almost any atoms where the 1s level is a "deep" core state (atoms heavier than carbon), the valence p states are largely delocalized and are hybridized with the surrounding atoms. A good description of these p states can only be given if the neighbors are taken into account. Then, a one-electron description, where p states are built from the neighbors and absorbing atom contributions and where correlations are not exactly treated (except through exchange and correlation one-electron potential), is the appropriate method for such edges. By construction, the multiple scattering framework is a suitable theory for obtaining information about the stereochemical arrangement around the absorber (bonding angles, three particles correlations, *etc.*[13]). The multiplet theory with Slater integrals determined by a Hartree–Fock program and developed in the crystal field formalism is a multielectronic calculation. It is well-suited to the $L_{2,3}$ edges of 3d transition metals that are transitions from the 2p core level to 3d states. Contrary to the metallic case, in coordination chemistry, the 3d states are very localized, almost atomic, except for the influence of the crystal field. The promotion of an electron on the 3d level completely modifies the energetic arrangement of the 3d levels; due to very large correlations, the photoelectron does not feel an effective one-electron potential but contributes to the building of the excited state. In this case, the correlations have to be treated exactly while the presence of the neighboring atoms is only introduced through the crystal field perturbation. Covalency is not treated and is supposed to be negligible. Therefore, the $L_{2,3}$ absorption edges are essentially sensitive to the local electronic structure of the absorber, and multiplet calculations can be used to gain information about the valency, symmetry, and magnitude of the crystal field acting on the 3d states of the absorber. To our knowledge, this paper is the first one that associates the two theoretical approaches with the same compound. It demonstrates clearly the origin of the modifications observed at both K and $L_{2,3}$ edges.

In Part I of this paper, we present the multiple scattering calculations performed at the iron K absorption edges of the $Fe^{II}(phen)_2(NCS)_2$ complex in both spin forms. The second part of this paper is devoted to the investigation of this complex at the iron $L_{2,3}$ edges and in particular to the crystal field multiplet simulations performed in this soft X-ray region. In each part, meaning for each kind of theoretical approach, results and discussion are given.

Experimental Section

Chemical Synthesis. Magnetic susceptibility measurements[4-7,10] on the $Fe^{II}(phen)_2(NCS)_2$ complex reveal that the spin transition is very dependent on the preparation method. One distinguishes two methods for preparing this complex. The first one, which is commonly called the "precipitation" method, leads to the formation of a complex characterized by a partial spin state interconversion.[6,7,10,14] The method labeled "extraction" is the one we used. Fully described in a previous paper,[3] it leads to a complex characterized by a complete and very abrupt high/low-spin interconversion at 176 K. The completeness of the spin transition is shown by the temperature dependence of the magnetic susceptibility χ_m presented in Figure 1 of ref 3. The difference in the magnetic behavior between samples obtained by either method is ascribed to differences in the size of crystallites.[6]

Data Collection. The experiments at the iron K edge were recorded at the Laboratoire pour l'Utilisation du Rayonnement Electromagnétique (LURE) Orsay, France, using the synchrotron radiation emitted by the DCI storage ring (λ_c = 3.5 Å) running at 1.85 GeV with an average current of 300 mA. The X-ray absorption spectra at the iron K edge were measured on the EXAFS IV station equipped with a double crystal Si(311) monochromator in transmission mode using ion chambers. The data were collected with a 1 s accumulation time per point and a stepwise of 0.25 eV. An oblong pellet of powdered materials was pressed, and the thickness was set in order to have a $\Delta\mu$ equal to 1.

The experiments at the iron $L_{2,3}$ edges have been recorded at the National Synchrotron Light Source (NSLS, Brookhaven, NY) on the Dragon U4-B beam line by collecting the total electron yield. Details about the resolution of the setup and sample preparation for the measurement are given in refs 3 and 15–17.

The spectra of a 7 μm iron metallic foil (at the K edge) or of Fe_2O_3 (at the L edges) were recorded immediately before and after each XANES spectrum to check energy calibration.

The measurements below the critical temperature of spin transition for the $Fe(phen)_2(NCS)_2$ complex at the K and L edges have been made at 77 K by using a liquid nitrogen cryostat. For each experiment, the sample temperature has been lowered at a rate of 2 K/min to avoid a quenching of the spin state. The reversibility of the process has been checked at the K and L edges by recording a spectrum after the total cycle (cooling and heating).

Data Processing. For K and $L_{2,3}$ edges, we subtract a linear background from the experimental spectra by extrapolating the least-square fitting of the pre-edge experimental points. At the K edge, we use as an energy reference the maximum of the first derivative in the iron metallic foil spectrum, corresponding to the first inflection point in the absorption curve (located at 7112 eV), and the edge jump determined by the EXAFS oscillation far from the edge is set to unity. At the $L_{2,3}$ edges, the energy calibration is chosen at the maximum of

(13) Di Cicco, A.; Filliponi, A. *J. Non-Cryst. Solids* **1993**, *156-158*, 102.

(14) Madeja, K.; Wilke, W.; Schmidt, S. *Z. Anorg. Allg. Chem.* **1966**, *346*, 306.

(15) Chen, C. T.; Sette, F. *Rev. Sci. Instrum.* **1989**, *60*, 1616.

(16) Chen, C. T.; Sette, F. *Phys. Scr.* **1990**, *T31*, 119.

(17) Sette, F.; Sinkovic, B.; Ma, Y. J.; Chen, C. T. *Phys. Rev. B* **1989**, *39*, 11125.

the L_3 line in Fe_2O_3 (708.5 eV), and the L edge spectra presented on the figures are arbitrarily normalized at 716 eV.

Part I: Multiple Scattering Calculations Performed at the Iron K Edge

To reproduce the changes observed at the iron K edge during the spin transition, full multiple scattering calculations have been performed using the computer codes developed by Natoli and co-workers and based on a real-space cluster method.[18,19] The multiple scattering method principally calculates the normalized photoelectron final state wave function as a solution to the Schrödinger equation for a muffin-tin potential. The X-ray absorption cross section has been calculated by application of the Golden rule.

We have used the crystallographic data from each spin state of the $Fe^{II}(phen)_2(NCS)_2$ complex synthesized by the "precipitation" method,[12] although our compound has been prepared by the "extraction" method. This choice has been justified by the fact that the single crystal X-ray diffraction investigation[12] is totally in agreement with the shortening of the Fe−N distances in the FeN_6 first coordination shell observed during the spin transition as first evidenced by EXAFS.[1] In addition, while it is well-known that the quality of the spin transition strongly depends on the method of preparation, no other difference in the performed characterizations has been detected between the samples prepared by different methods[7] (for instance, powder diffraction patterns[8] and iron K edge absorption spectra[20] of both samples are identical).

During the spin transition, the space group P_{bcn} (D_{2h}^{14}) of the molecule remains unchanged, and the arrangement of the $Fe^{II}(phen)_2(NCS)_2$ units is quite the same in both spin forms. The most important change lies in the intramolecular geometry, in particular the shortening of the Fe−N distances in the first coordination shell around the iron. For the low-spin form[12] and the high-spin form, the iron is surrounded by four nitrogen atoms of the two 1,10-phenanthroline ligands at 2.01 and 2.20 Å, respectively, and two nitrogen atoms of the two thiocyanate groups in cis positions at 1.96 and 2.06 Å, respectively.

Insofar as the structural changes observed during the spin conversion are essentially intramolecular, the cluster size for the multiple scattering calculation is set to a whole molecular unit (35 atoms) with the absorbing iron atom at the center ("spherical" cluster with a radius of 6.1 Å). Although the carbon atoms of the phenanthroline groups belonging to neighboring molecular units happen to be closer to the iron-absorbing atom than the farthest atoms of the absorbing atom molecular unit, these extramolecular atoms are not considered in the cluster. Indeed, they are not involved in any focusing effect that might enhance their contribution.

The potentials of the ground and excited states are of the muffin-tin type, and their construction has been described previously[19] using the Norman criterium for the choice of the muffin-tin radii.[21] The latter are gathered for both spin states in Table 1. We used Clementi and Roetti SCF atomic tabulated values to generate atomic charge densities.[22] A "muffin-tin" potential has been calculated in the X-α approximation with the Schwartz prescription for α coefficients.[23] The molecular potentials have been calculated without overlap between atomic spheres of the cluster.

Table 1. Muffin-Tin Radii (Å) of the 18 Prototypical Atoms of the Molecular Cluster Obtained for Each Spin State[a]

prototypical atoms	low-spin form	high-spin form
outer sphere	5.947	6.118
Fe (ground state)	1.152	1.230
Fe (excited state)	1.152	1.262
N(1)	0.580	0.581
N(2)	0.649	0.658
N(20)	0.660	0.653
C(1)	0.684	0.683
C(2)	0.686	0.679
C(3)	0.690	0.679
C(21)	0.681	0.576
C(12)	0.574	0.674
C(6)	0.682	0.679
C(9)	0.713	0.688
C(4)	0.693	0.690
C(11)	0.689	0.682
S(22)	0.994	0.967
C(5)	0.689	0.690
C(10)	0.693	0.682
C(7)	0.680	0.680
C(8)	0.680	0.680

[a] The numbering of atoms is the one given in Table II of the ref 12.

The influence of the electronic configuration of the excited state on the molecular potentials has been tested. The best simulation has been obtained for the so-called "relaxed and screened" excited state potential; the iron orbitals with a 1s core hole are estimated to be similar to ground state cobalt orbitals [(Z + 1) approximation: 26 protons + ($1s^1 2s^2 2p^6 3s^2 3p^6 4s^2 3d^{6+1}$) configuration]. The extra electron in the 3d shell accounts for some screening of the attractive core hole potential.

For both spin states of the $Fe^{II}(phen)_2(NCS)_2$ complex, the full point group of the P_{bcn} space group is D_{2h}, which confers to the dipole K edge absorption cross section a trichroic dependence (three independent parameters σ_x, σ_y, and σ_z).[24] The local point group of iron atoms is C_2 (trichroism with four parameters[24]), and there are four iron atoms per unit cell. The isotropic spectrum in the electric dipole approximation can be exactly computed by $3\sigma_{iso} = \sigma_x + \sigma_y + \sigma_z$ (where $\hat{x} \perp \hat{y}$, $\hat{x} \perp \hat{z}$, and $\hat{y} \perp \hat{z}$).

We have taken into account the C_2 symmetry of the local point group of the absorbing atom in the cluster. The use of symmetry arguments reduces the number of independent atoms in the cluster to 18 nonequivalent atoms, which means the other ones are obtained by applying the two symmetry operations of the C_2 point group. The C_2 rotation axis is parallel to the y direction. Convergence for the l expansion in the angular momentum basis has been checked, and terms lower than $l_{max} = 5$ have been retained.

The theoretical spectra presented for both complexes have been convolved by an energy-dependent Lorentzian broadening function whose width, Γ_{tot}, is given by $\Gamma_{tot}(E) = \Gamma_h + \Gamma_{exp} + \Gamma_{el}(E)$ where Γ_h is the core-hole width (Γ_h = 1.25 eV[25]) and Γ_{exp} is the full experimental resolution (divergence of the beam, rocking curve width). The sum $\Gamma_h + \Gamma_{exp}$ is taken equal to 1.9 eV. $\Gamma_{el}(E)$ is a varying energy-dependent damping function related to the mean-free path of the photoelectron in the final state determined by inelastic losses of the scattered photoelectron. It reads

$$\Gamma_{el}(E) = \frac{\hbar}{\lambda(E)}\sqrt{\frac{2E}{m}} \quad \text{and} \quad \lambda(E) = \frac{k}{\mathrm{Im}\Sigma(r,E)}$$

where Σ is the self-energy of the photoelectron.

(18) Kutzler, F. W.; Natoli, C. R.; Misemer, D. K.; Doniach, S.; Hodgson, K. O. *J. Chem. Phys.* **1980**, *73*, 3274.
(19) Natoli, C. R.; Misemer, D. K.; Doniach, S.; Kutzler, F. W. *Phys. Rev. A* **1980**, *22*, 1104.
(20) Roux, C. Ph.D. Thesis, University of Paris-Sud, 1992.
(21) Norman, D. *Phys. Rev. Lett.* **1983**, *51*, 2052.
(22) Clementi, E.; Roetti, C. *At. Data Nucl. Data Tables* **1974**, *14*, 177.
(23) Schwartz, K. *Phys. Rev. B* **1972**, *5*, 2466.
(24) Brouder, C. *J. Phys.: Condens. Matter* **1990**, *2*, 701.
(25) Krause, M. O.; Oliver, J. H. *J. Phys. Chem. Ref. Data* **1979**, *8*, 32.

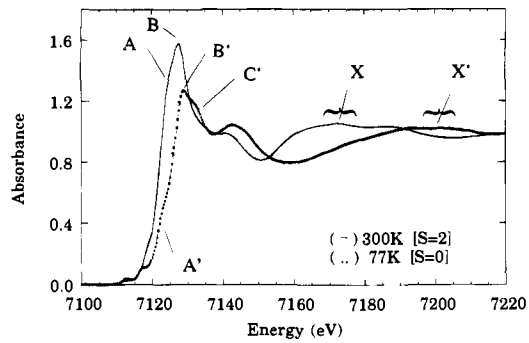

Figure 1. XANES experimental spectra recorded on the spin transition $Fe(phen)_2(NCS)_2$ complex at the iron K edge. The solid line shows the high-spin isomer recorded at 300 K, and the dotted line shows the low-spin isomer recorded at 77 K.

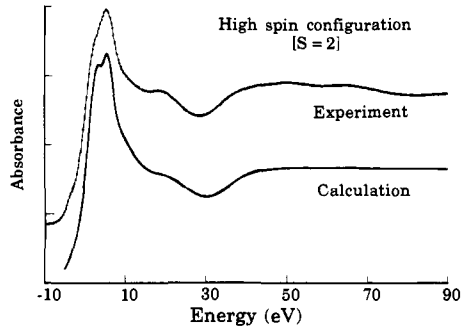

Figure 2. Comparison between K edge experimental and X-α calculated spectra (multiple scattering framework) for the high-spin $Fe(phen)_2(NCS)_2$ isomer. The calculated curve has been convolved with an energy-dependent Lorentzian broadening function.

Results and Discussion

As can be seen on XANES experimental spectra recorded at the iron K edge (Figure 1), the modifications during the spin crossover of the $Fe(phen)_2(NCS)_2$ complex are large. One observes that during the transition from high- to low-spin configurations, the intensity of the shoulder labeled A in the main rising edge (7125 eV) is strongly reduced to the shoulder labeled A′. The white line (7127 eV) labeled B is shifted toward higher energy in B′ (7130 eV), and a new shoulder labeled C′ (7133 eV) appears. The large bump labeled X (around 7170 eV) in the high-spin spectrum corresponds to the X′ resonance (around 7190 eV) in the low-spin spectrum. X and X′ energies can be easily related by Natoli's well-known rule[26] that states that Ed^2 = cste, where E is the resonance energy relative to a given zero energy and d is the mean distance of the Fe−N bound in the compounds. If the zero energy is chosen as the first unoccupied state, the ratio of the energies in both isomers is 0.9. This corresponds to the contraction of the average iron−nitrogen distance (ratio = 0.9) in the first iron coordination shell and not to the average variation of the unit cell parameters (ratio = 0.98). This clearly shows that the spectra regions 50 eV above the edge are mainly governed by the first coordination shell and that intermolecular interactions are negligible.

Figures 2 and 3 show the comparison between experimental and calculated spectra for both spin states of the $Fe^{II}(phen)_2(NCS)_2$ complex. The agreement between both experimental and calculated spectra is good.

The multiple scattering calculations effectively reproduce the sensitivity of the K edges to the nature of the 4p(metal) antibonding levels. Namely, from Figures 2 and 3, we note that calculations effectively account for the decrease of the

(26) Natoli, C. R.; Benfatto, M.; Doniach, S. *Phys. Rev. A* **1986**, *34*, 4682.

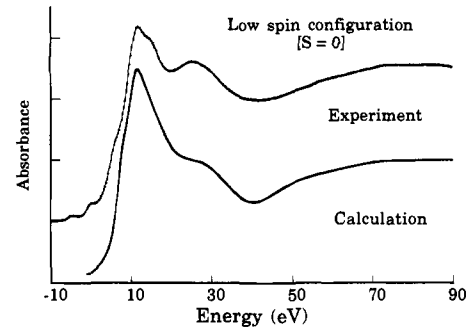

Figure 3. Comparison between K edge experimental and X-α calculated spectra (multiple scattering framework) for the low-spin $Fe(phen)_2(NCS)_2$ isomer. The calculated curve has been convolved with an energy-dependent Lorentzian broadening function.

amplitude of the white line. We note that the A′ resonance in Figure 3 is not reproduced with the correct energy and intensity compared to the experiment. Nevertheless, the trends between A and A′ resonances during spin conversion are present in the calculation where A′ is shifted toward lower energy and has a lower intensity. The C′ resonance is almost not present in the calculation where it appears as a broadening of the white line on its high-energy side. The main resonances (A, B or A′, B′) can be understood as originating from a transition toward antibonding states that results from hybridization between N(2p) and Fe(4s,4p) states. During the transition from the high-spin to the low-spin complex, the Fe−N distances are shortened. Consequently, the hybridization is enhanced, leading to the following trends: (i) the antibonding state N(2p)−Fe(4s,4p) is pushed toward higher energies (on the experimental and theoretical spectra, the shift is ≈ 3 eV for the maximum) and (ii) the mixing of the ligands N(2p) with the metal Fe(4s,4p) is stronger in the antibonding state, and then there is a decrease in the Fe density of the empty states, and the resonance is weaker in the low-spin spectrum than in the high-spin one. We note that the calculations are able to reproduce qualitatively the energy shift and the intensity variation observed experimentally during the spin transition.

It can be seen in Figures 2 and 3 that the main modifications originate from the shortening of iron−ligand distances and the subsequent rearrangements of the molecule occurring during the spin transition. Therefore, modifications of the calculated spectra can be considered as originating only from intramolecular structural changes and not from electronic correlations in the 3d states. No special attention has been given to the spin configuration of atomic iron in the potential construction. This choice was first motivated by the fact that the potential differences between two spin configurations are liable to be smeared out by the spherical averaging inside an iron atomic sphere. Second, these modifications are much less important than those produced by the potential of nitrogen atoms whose tails overlap the iron atomic potential.

In the pre-edge region, the agreement is not perfect because the zero energy used in the multiple scattering calculation is equal to the interstitial potential and not to the energy of the vacuum. Then, the states between the Fermi level and the vacuum level are not treated like bound states but like states of the continuum. This approximation proves to be too crude for these levels. Moreover, this region just above the Fermi level depends greatly on the choice of muffin-tin sphere radii, either overlapping percentage or Norman or Wille criteria.[21] Except for the calculation without "muffin-tin" approximation, a parameter-free solution for the potential construction does not exist.

Part II: Crystal Field Multiplet Calculations Performed at the Iron L Edges

The atomic absorption at $L_{2,3}$ edges of 3d transition metals involves electric dipole transitions from a 2p core electron to incompletely filled 3d and 4s levels. In this paper, the 2p → 4s transitions are neglected due to their low intensity relative to the 2p → 3d transitions. The positions of the multiplet structures observed at $L_{2,3}$ edges are the final state energies arising from Coulomb interaction within the 3d shell and between 2p and 3d shells, from spin−orbit interaction on the 2p and 3d shells, and from crystal field on the 3d shell. The crystal field multiplet framework is based on the calculation of the energy of the electronic states of the absorber imbedded in the crystal field potential produced by the ligands. The important parameters of such calculations are (i) the nature of the absorbing atom, and in particular, the occupancy of the valence orbitals, (ii) the local symmetry around the absorber, and (iii) the strength of the crystal field. The absorber−ligand distances and the chemical nature of the ligands are not given explicitly in this kind of calculation. In fact, structural and chemical information enters indirectly into the multiplet calculation in the form of the crystal field strength and of the value of the κ parameter, which scales the atomic values of Slater integrals. In our calculations, the κ parameter is chosen as 80% according to the value prescribed by Cowan.[27,28]

The method of crystal field multiplet calculation has been described by Thole and co-workers in many papers.[29−34] At first, the initial and final state basis functions are determined using Cowan's programs.[27,28] These basis functions are calculated *ab initio* within the Hartree−Fock approximation. Then, the reduced matrix elements of the Coulomb, spin−orbit, and electric dipole operators are calculated in the spherical O_3 group. Finally, the calculations in crystal field symmetry are performed using the group theory approach of Butler.[35,36]

The symmetry of the crystal field perturbation is C_2. It results from the ordering of nitrogen atoms around iron. Eight parameters would be necessary to describe such a ligand field. Since the local environment of iron is approximately octahedral (the deviation from O_h symmetry is smaller in the low-spin form than in the high-spin one[12]), the crystal field perturbation has been taken to be octahedral. In the O_h approximation, the only free parameter to reproduce the experimental spectra is the $10Dq$ crystal field strength, which represents, before spin−orbit and Coulomb interactions are turned on, the splitting of the 5-fold degenerate 3d orbitals into two orbital groups of e_g and t_{2g} symmetry with 2-fold and 3-fold degeneracy, respectively. Other parameters like the Slater integrals, which take into account the Coulomb interactions within the 3d shell for the ground state, within the 3d shell and between the 2p and 3d shells in the excited state and of the 2p and 3d spin−orbit interactions are *ab initio* values obtained from Cowan's programs.[27,28] They are the same for all calculations and are gathered in Table 2. Due to electron correlation effects, these Slater integrals were reduced in our calculations by 80% (κ factor).

Table 2. Parameters (eV) for the Ground and Excited State Configurations

state	F^2(d,d)	F^4(d,d)	ζ(2p)	ζ(3d)	F^2(p,d)	G^1(p,d)	G^3(p,d)
ground Fe $3d^6$	8.773	5.452		0.052			
excited Fe $2p^53d^7$	9.423	5.862	8.200	0.067	5.434	4.003	2.275

The calculated line spectra were convolved with a Gaussian profile with a full width at half-maximum (fwhm) σ for L_3 and L_2 edges and with a Lorentzian profile with a fwhm Γ_1 for the L_3 edge and Γ_2 for the L_2 one. The convolution with the Gaussian profile represents instrumental broadening, the value of σ being taken as the energy resolution value expected with the Dragon monochromator for the energy range of the Fe $L_{2,3}$ edges[37] and for the used slits width.[3] The Lorentzian broadening represents the lifetime width of the core hole. The Γ_2 value, relative to the L_2 part of the 2p spectrum, is higher than the Γ_1 value given for the L_3 one because of the opening of Coster−Kronig Auger decay channels.[38]

In order to facilitate comparison between experimental and calculated spectra, the intensity of the maximum of the L_3-calculated spectra has been normalized to one.

Results and Discussion

In contrast to the poor information relative to the filling of the 3d states, which can be extracted from the K edge study, it is well-known[3,30,39−44] that the $L_{2,3}$ transition metal edges are a good fingerprint of the spin state because of the very restrictive electric dipole selection rules, the main dipole-allowed transition being 2p → 3d and with a weaker 2p → 4s probability. Furthermore, the core hole lifetime being longer than at the K edge, more experimental structures can be resolved in $L_{2,3}$ spectra. With the new generation of soft X-ray monochromators like the AT&T Bell Lab Dragon,[15−17] a better experimental resolution is available and offers new insight into the study of 3d transition metal compounds.

Figures 4 and 5 show the results of the multiplet calculations compared to the experimental spectra recorded at the iron $L_{2,3}$ edges for the $Fe^{II}(phen)_2(NCS)_2$ complex above and below the T_c temperature of spin conversion. The $10Dq$ crystal field strength for both spin states is optimized and found to be 0.5 eV for the high-spin configuration (Figure 4) and 2.2 eV for the low-spin one (Figure 5).

In these figures, we have also reported individual lines representing the transition probability. The line spectra are the raw results of multiplet calculations. But to compare them with the experimental spectra, they have to be broadened as described

(27) Cowan, R. D. *The Theory of Atomic Structure and Spectra;* University of California Press: Berkeley, 1981.
(28) Cowan, R. D. *J. Opt. Soc. Am.* **1968**, *58*, 808.
(29) Thole, B. T.; Cowan, R. D.; Sawatzky, G. A.; Fink, J.; Fuggle, J. C. *Phys. Rev. B* **1985**, *31*, 6856.
(30) Thole, B. T.; van der Laan, G.; Butler, P. H. *Chem. Phys. Lett.* **1988**, *149*, 295.
(31) de Groot, F. M. F.; Fuggle, J. C.; Thole, B. T.; Sawatzky, G. A. *Phys. Rev. B* **1990**, *41*, 928.
(32) de Groot, F. M. F.; Fuggle, J. C.; Thole, B. T.; Sawatzky, G. A. *Phys. Rev. B* **1990**, *42*, 5459.
(33) van der Laan, G.; Kirkman, I. W. *J. Phys.: Condens. Matter* **1992**, *4*, 4189.
(34) de Groot, F. M. F. *J. Electron Spectrosc. Relat. Phenom.* **1993**, *62*, 111.
(35) Butler, P. H. *Point Group Symmetry, Applications, Methods and Tables*; Plenum: New York, 1991.
(36) Butler, P. H.; Wybourne, B. G. *Int. J. Quantum Chem.* **1976**, *10*, 581.
(37) Chen, C. T. *Nucl. Instrum. Methods Phys. Res., Sect. A* **1987**, *256*, 595.
(38) Pease, D. M. *Phys. Rev. B* **1991**, *44*, 6708.
(39) van der Laan, G.; Thole, B. T.; Sawatzky, G. A.; Verdaguer, M. *Phys. Rev. B* **1988**, *37*, 6587.
(40) Thole, B. T.; van der Laan, G. *Phys. Rev. B* **1988**, *38*, 3158.
(41) Cramer, S. P.; de Groot, F. M. F.; Ma, Y.; Chen, C. T.; Sette, F.; Kipke, C. A.; Eichhorn, D. M.; Chan, M. K.; Armstrong, W. H.; Libby, E.; Christou, G.; Brooker, S.; McKee, V.; Mullins, O. C.; Fuggle, J. C. *J. Am. Chem. Soc.* **1991**, *113*, 7937.
(42) Cartier, C.; Flank, A. M. *X-Ray Absorption Fine Structure*; York, S. S., Ed.; Ellis Horwood Publishers: Chichester, U.K., 1991; p 659.
(43) George, S. J.; van Elp, J.; Chen, J.; Ma, Y.; Chen, C. T.; Park, J.-B.; Adams, M. W. W.; Searle, B. G.; de Groot, F. M. F.; Fuggle, J. C.; Cramer, S. P. *J. Am. Chem. Soc.* **1992**, *114*, 4427.
(44) van Elp, J.; Peng, G.; Searle, B. G.; Mitra-Kirtley, S.; Huang, Y.-H.; Johnson, M. K.; Zhou, Z. H.; Adams, M. W. W.; Maroney, M. J.; Cramer, S. P. *J. Am. Chem. Soc.* **1994**, *116*, 1918.

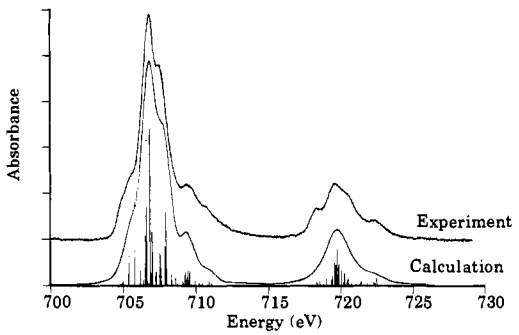

Figure 4. Comparison between experimental and calculated ($3d^6$ to $2p^53d^7$ multiplet) $L_{2,3}$ edge spectra for the high-spin $Fe(phen)_2(NCS)_2$ isomer. Calculation is made considering O_h symmetry with a $10Dq$ cubic crystal field parameter equal to 0.5 eV.

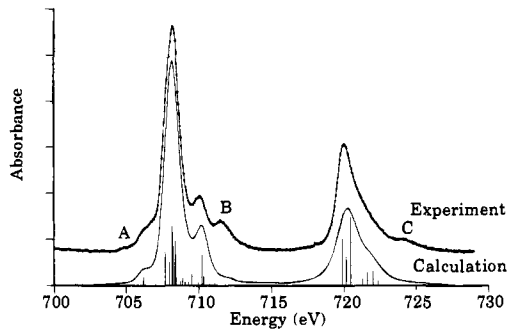

Figure 5. Comparison between experimental and calculated ($3d^6$ to $2p^53d^7$ multiplet) $L_{2,3}$ edge spectra for the low-spin $Fe(phen)_2(NCS)_2$ isomer. Calculation is made considering O_h symmetry with a $10Dq$ cubic crystal field parameter equal to 2.2 eV.

above. These broadening calculations are done by trial and error, not by an automatic fitting procedure; one σ and Γ fwhm parameters set that seems to fit the best has been obtained within the limit of expected core hole and experimental broadenings, which are $\sigma = 0.125$ eV, $\Gamma_1 = 0.1$ eV, and $\Gamma_2 = 0.3$ eV. This broadening description, as Voigt profiles (Lorentzian-convolved by Gaussian profiles) for the L_3 and L_2 edges, is very rough because it assumes that effects on the spectral shapes such as lifetime, hybridization, and vibration are the same for all final multiplet lines. Since previous work[32] showed some disagreement with this approach for d^0 compounds, we can expect similar results for $3d^6$ compounds.

Nevertheless, despite the difficulty in the determination of the broadening parameters, the agreement between calculated and experimental spectra can be considered satisfactory because it reproduces the main experimental changes observed during the spin transition. Below the spin transition temperature, sharper structures at the L_3 edge appear and the L_2 white line increases strongly in intensity.

All features observed for the high-spin form are well-reproduced (Figure 4). Therefore, although the iron site symmetry for the high-spin isomer is far from an octahedron, the O_h crystal field approach gives a good description of all spectral details presented in Figure 4. The agreement for the low-spin one (Figure 5) is not so good. Indeed, the very small peaks (A) at the low-energy side of the L_3 edge and (C) at the high-energy side of the L_2 edge are not reproduced in the calculated spectrum. Furthermore, the intensity of the calculated peak (B) at the high-energy side of the L_3 edge is too low and not very well located in energy. The small disagreement between the experimental spectra of the $Fe^{II}(phen)_2(NCS)_2$ complex and the octahedral symmetry simulation can be ascribed to a distorsion of the iron site and/or to hybridization between the metal 3d orbitals and the (NCS) ligands,[45,46] which was not taken into account in our calculations.

Table 3. Dominant Components (>1%) of Each Basis That Transforms as the T_{2g} and A_{1g} Irreps of the O_h Point Group

irrep T_{2g} at $10Dq = 0.5$ eV		irrep A_{1g} at $10Dq = 2.2$ eV	
$^5D_{J=2}$	2.6%	$^1S_{J=0}$	3.7%
$^5D_{J=3}$	16.2%	$^1S_{J=0}$	5.8%
$^5D_{J=4}$	81.2%	$^1G_{J=4}$	31.2%
		$^1G_{J=4}$	21.8%
		$^1I_{J=6}$	36.2%

Beyond the agreement between experiments and calculations and the determination of the $10Dq$ parameter, the multiplet approach offers new insight into the knowledge of the ground state of the materials. We can understand, for each spin state, the values of $\langle S\rangle$ and $\langle L\rangle$[47] and the ground state energy.

Interesting average values such as $\langle S\rangle$ and $\langle L\rangle$[47] can be calculated. The $\langle S\rangle$ values obtained for $10Dq = 0.5$ eV and $10Dq = 2.2$ eV are 1.999 and 0.0266, respectively, meaning that the spin states in each spin form of the $Fe^{II}(phen)_2(NCS)_2$ complex are very pure, minor differences with pure singlet or quintet spin states being due to the introduction of spin–orbit interaction, which makes $\langle S\rangle$ a bad quantum number. Below the $10Dq$ spin conversion value, the angular momentum $\langle L\rangle$ is constant and equal to 2. Above the $10Dq$ spin conversion value, $\langle L\rangle$ decreases slowly from 4.6.

We have access to a precise determination of the ground state. It can be decomposed on the basis of the *LS* vectors associated, in the considered point group, with the $3d^6$ configuration.[27] During the spin conversion, the O_h irreducible representation (irrep) of the ground state changes. For the high-spin state, it is the T_{2g} irrep;[48] for the low-spin form, it is the A_{1g} irrep.[48] In the case of the high-spin form, the ground state corresponding to the $3d^6$ configuration in octahedral symmetry is obtained by mixing 27 basis vectors. But for the low-spin form, the ground state is a mixture of only 14 basis vectors (there are a number of ways to branch the *LSJ* terms of $3d^6$ to T_{2g} and A_{1g}, respectively). Although the nature of this ground state can be properly specified only by giving the complete basis function expansion, some components are clearly dominant in these mixtures. We have reported in Table 3 the weight of the dominant components in each mixture.

For a small $10Dq$, the dominant eigenvector is $^5D_{J=4}$ with $\langle S\rangle = 2$ spin as expected from Hund's rules. For the low-spin state, the dominant eigenvectors are $2(^1S_{J=0})$, $2(^1G_{J=4})$, and $^1I_{J=6}$

(45) Jo, T.; Sawatzky, G. A. *Phys. Rev. B* **1991**, *43*, 8771.

(46) van der Laan, G.; Thole, B. T. *J. Phys.: Condens. Matter* **1992**, *4*, 4181.

(47) $\langle S\rangle$ is such that $\langle S\rangle(\langle S\rangle + 1)\hbar^2 = \langle \text{Ground} \mid S_x^2 + S_y^2 + S_z^2 \mid \text{Ground}\rangle$ where

$$\vec{\mathbf{S}} = \begin{pmatrix} S_x \\ S_y \\ S_z \end{pmatrix}$$

is the spin momentum operator. $\langle L\rangle$ is such that $\langle L\rangle(\langle L\rangle + 1)\hbar^2 = \langle \text{Ground} \mid L_x^2 + L_y^2 + L_z^2 \mid \text{Ground}\rangle$ where

$$\vec{\mathbf{L}} = \begin{pmatrix} L_x \\ L_y \\ L_z \end{pmatrix}$$

is the orbital momentum operator, $\langle L\rangle$ should not be confused with $\langle L_z\rangle = \langle \text{Ground} \mid L_z \mid \text{Ground}\rangle$.

(48) For high-spin configuration after crystal field splitting, the ground state is $^5T_{2g}$ (15-fold) that splits into T_{2g} (3-fold) under spin–orbit coupling. It is to this T_{2g} that we refer, and similar definition for low-spin A_{1g}. These T_{2g} and A_{1g} ground states are constructed from several $|LSJM\rangle$ states because of spin–orbit interaction.

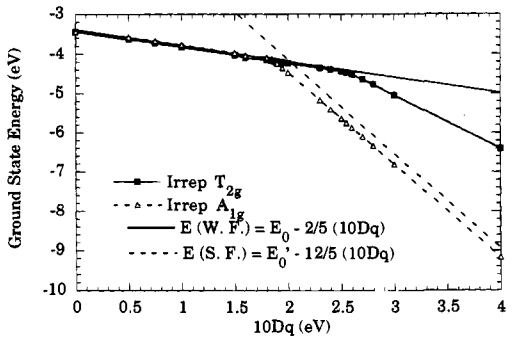

Figure 6. Variation of the energy of the ground state of both irreps T_{2g} and A_{1g} as a function of the $10Dq$ crystal field parameter compared to the variation of the energies E(WF) and E(SF) obtained by König *et al.*[50-53] in the weak field and strong field approaches with F^2 (dd) = 8.773 eV and F^4(dd) = 5.452 eV, respectively.

with $\langle S \rangle = 0$.[49] The same analysis shows that the average orbital momentum is $\langle L \rangle = 2$ for the high-spin state and $\langle L \rangle \approx 4.6$ for the low-spin state, which is a mixture of $L = 4$ and $L = 6$.

The evolution of the energies of the ground states T_{2g} and A_{1g} as a function of $10Dq$ is shown in Figure 6 where we observe clearly two kinds of variations. Below the spin transition, *i.e.*, $10Dq < 1.85$ eV, the difference between the ground state energies of the T_{2g} and A_{1g} irreps is very small. The gap between the states' energy of symmetry of A_{1g} and T_{2g} corresponds to the spin–orbit coupling parameter ζ_{3d}. Above the spin transition, *i.e.*, $10Dq > 2.0$ eV, the ground state energy of A_{1g} irrep is clearly much lower than the energy of the T_{2g} state.

The $10Dq$ dependence of the ground state energy has been investigated by König and Kremer[50-53] in octahedral transition metal complexes. Since 3d spin–orbit coupling is small (ζ_{3d} = 0.052 eV), we can neglect it and have a simpler physical picture. The energy depends on Coulomb and crystal field interactions. In the weak (strong) field regime, crystal field interaction is smaller (greater) than Coulomb interaction. König *et al.*[50-53] have established the $10Dq$ dependence of the ground energy in the weak field (1) and the strong field (2) regimes:

$$E(\mathrm{WF}) = -\,{}^{5}/_{21}[F^2(\mathrm{d,d}) + F^4(\mathrm{d,d})] - {}^{2}/_{5}(10Dq) \quad (1)$$

$$E(\mathrm{SF}) = -\,{}^{20}/_{147}F^2(\mathrm{d,d}) + {}^{50}/_{147}F^4(\mathrm{d,d}) - {}^{12}/_{5}(10Dq) \quad (2)$$

Figure 6 displays these two functions and shows that the high-spin state of the weak field regime is very close to $|^5\mathrm{D}\ ^5\mathrm{T}_{2g}\rangle$. However, the molecular orbital picture of the strong field regime (Figure 7) is not so good for the low-spin state, which is not a pure $|(t_{2g})^6\ ^1\mathrm{A}_{1g}\rangle$. This is confirmed by the calculation of the orbital momentum $\langle (t_{2g})^6 | L_x^2 + L_y^2 + L_z^2 | (t_{2g})^6 \rangle = 24$ (so that $\langle L \rangle \approx 4.4$ instead of 4.6).

Finally, in Table 4 we compare the $10Dq$ values that gave the best simulations with parameters derived from UV–visible spectroscopy[4] for both complexes.

We observe that the $10Dq$ values obtained from multiplet calculations on the low-spin form and from UV–visible spectroscopy are close in magnitude, whereas there is a large discrepancy between both $10Dq$ values of the high-spin form. Such discrepancies on high-spin manganese(II) complexes have already been noticed by Cramer *et al.*[41] Their argument to explain it is that the $10Dq$ values extracted from X-ray absorption spectroscopy are not ground state $10Dq$ values but final state values where the 3d states react toward the presence of the 2p core hole. In fact, in the calculations, two $10Dq$ parameters are needed, one for the ground state ($10Dq_{GS}$) and the other for the excited state ($10Dq_{ES}$). When the 3d spin–orbit coupling is negligible, if the ground state is made of only one *LS* term, which is the case for all high-spin transition metals, it can be shown that the spectrum is not sensitive to the crystal field strength in the ground state. Indeed, the ground state is completely determined by the ground state irrep. We have verified that, by using $10Dq_{GS}$ = 1.49 eV and $10Dq_{ES}$ = 0.5 eV, the calculated spectrum is similar to the one with $10Dq_{GS}$ = $10Dq_{ES}$ = 0.5 eV. This means that, for high-spin complexes, X-ray absorption spectroscopy is not sensitive to the ground state $10Dq$ but only to the excited state one. On the other hand, low-spin states are made of many *LS* terms that are mixed by the crystal field, and the spectra are sensitive to both initial and final $10Dq$. To understand this one should notice that, if the spin–orbit coupling is neglected, there is only one high-spin term for transition metals (for Fe^{2+}, the only $S = 2$ term is $L = 2$). Since the crystal field does not mix *LS* terms with different *S* terms, the high-spin molecular states remain within the high-spin atomic term. In the example of Fe^{2+}, the ^{5}D term is split by the octahedral crystal field into $^5T_{2g}$ and ^5E_g. Once the irrep is chosen ($^5T_{2g}$), the expansion of the $^5T_{2g}$ states over the ^{5}D basis functions is fully determined (and can be found, for instance, in ref 35). Changing the crystal field value does not modify this expansion or, in other words, the ground state is not changed by the crystal field strength once the ground irrep is chosen. This is why the spectrum is not sensitive to the crystal field values of the ground state of a high-spin complex. The presence of spin–orbit coupling can modify this conclusion, but we have checked that this was not the case for high-spin Fe(II) compounds. On the other hand, in low-spin complexes, there are many basis states for irrep $^1A_{1g}$, and the crystal field strength determines the amount of each basis state in the ground state. The resulting spectrum is strongly dependent on the ground state $10Dq$.

Conclusion

In this paper, we have studied and enhanced the comprehension of the electronic structure of a spin transition 3d molecular compound. These compounds have received much interest in the coordination chemistry community.[4-12,54-59] We have particularly addressed two phenomena that determine the electronic structure during the spin transition: the variation of the 3d electronic configuration and the atomic rearrangement. With this paper, we have shown that it is possible to characterize both phenomena by using only one spectroscopy. X-ray absorption spectroscopy is angular momentum selective, and by changing the excitation energy, one probes vacant states of different symmetry in a given atom. At the K absorption edge of the metal, transitions to p states occur and the XANES part is very sensitive to the atomic arrangement. Performing multiple scattering calculations, we have shown that the main modifications of the XANES originate only in the subsequent rearrangement of the molecule occurring during the spin transition. In the $L_{2,3}$ absorption edges, transitions to very localized 3d states occur and reflect the electronic structure. The XANES modi-

(49) Before the parenthesis is indicated the number of different terms having the same values of *LS*.

(50) König, E.; Kremer, S. *Theor. Chim. Acta* **1971**, *22*, 45.
(51) König, E.; Kremer, S. *Theor. Chim. Acta* **1971**, *23*, 12.
(52) König, E.; Kremer, S. *Z. Naturforsch.* **1974**, *29A*, 31.
(53) König, E.; Kremer, S. *Ligand Field Energy Diagrams*; Plenum Press: New York, 1977.
(54) König, E.; Ritter, G.; Kulshreshtha, S. K.; *Chem. Rev.* **1985**, *85*, 219.
(55) König, E. *Prg. Inorg. Chem.* **1987**, *35*, 527.
(56) Rao, C. N. R. *Int. Rev. Phys. Chem.* **1985**, *4*, 19.
(57) König, E. *Struct. Bonding (Berlin)* **1991**, *76*, 51.
(58) Goodwin, H. A. *Coord. Chem. Rev.* **1976**, *18*, 293.
(59) Zarembowitch, J. *New J. Chem.* **1992**, *16*, 275.

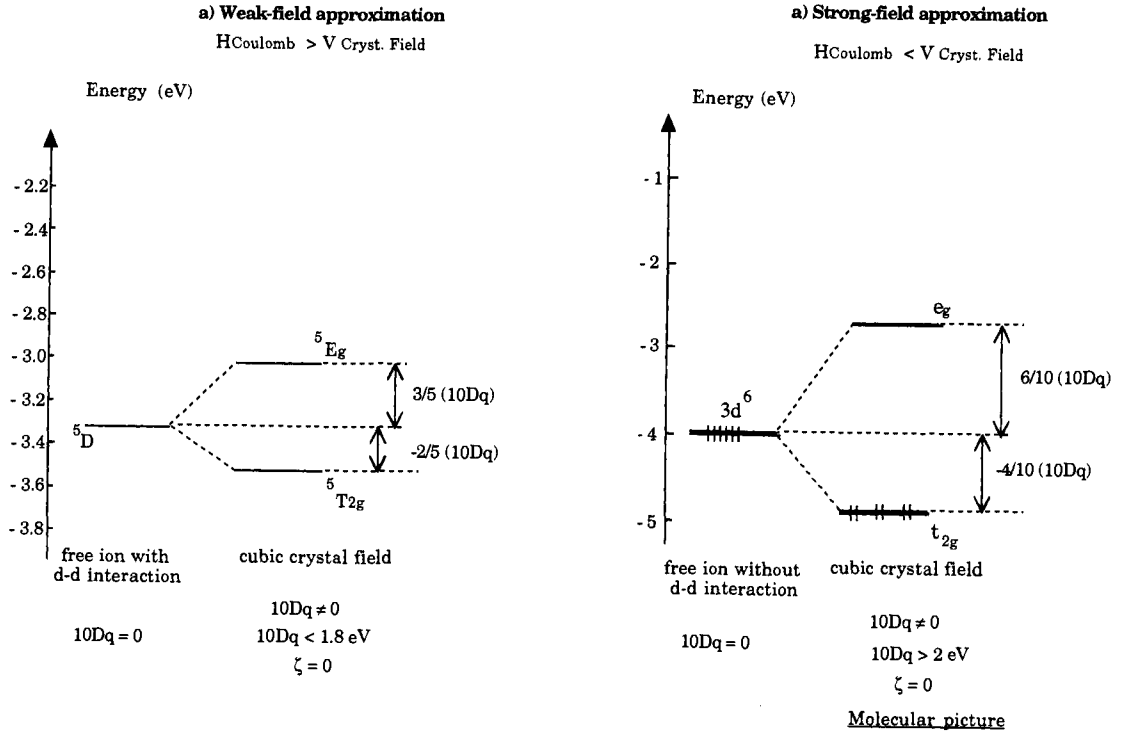

Figure 7. Simplified energy diagram established in the weak field approximation (left) and the strong field approximation (right). The energies are relative to the average energy of the $3d^6$ configuration.

Table 4. Comparison of the 10*Dq* Values Giving the Best Multiplet Simulations at the L Edges with the Parameters Deduced from UV−Visible Spectroscopy

compound	spin form	10*Dq* (UV−visible)[4]	10*Dq* (this work)
$Fe(phen)_2(NCS)_2$	high-spin	11 900 cm^{-1}, *i.e.*, 1.49 eV	0.5 eV
$Fe(phen)_2(NCS)_2$	low-spin	16 300 cm^{-1}, *i.e.*, 2.04 eV	2.2 eV

fications observed during spin transition can be associated with a change in the occupancy of the 3d levels. There is no unifying code available to calculate both delocalized and localized final states. When correlations are important as in narrow bands like 3d bands, multiplet calculations are expected to be the correct method. In this formalism, the nature of the surrounding atoms is not taken into account in a straightforward way. This limits its application to compounds with weak hybridization. When correlations are expected to be small, as in the case of delocalized p states of the continuum, the multiple scattering technique is the suitable method for describing X-ray absorption spectra. In this technique, the neighbors are correctly taken into account through their scattering phase shifts and their crystallographic positions around the absorbing atom.

Finally, we point out that the multiplet approach used to simulate experimental $L_{2,3}$ edges of 3d transition metals gives a precise description of the ground state. The precise knowledge of the ground state can be used in other theoretical models to give an interpretation of the unusual magnetic properties exhibited by spin transition molecules.[50−53,60,61] The magnetic behavior is governed by two factors, the magnitude of the ligand field parameter 10*Dq* and its variation with temperature. We show that the multiplet calculations allow us to address these values. The 10*Dq* values extracted from X-ray absorption spectroscopy have to be compared to those derived from UV−visible spectroscopy. The 10*Dq* values measured by both methods are related to a different excited state, and complementary information is gained. By using the atom selectivity of the X-ray absorption spectroscopy, it is also possible to measure the local magnetic moments for each atomic species. This new tool should be extremely interesting in the case of new molecular magnets.[62−68]

Combining different edges, X-ray absorption spectroscopy is a powerful tool for characterizing electronic and structural properties of various materials, particularly those presenting evolutions under external perturbations[54−59] or containing active centers in biomaterials.[43,44,69−73]

Acknowledgment. We acknowledge the help of C. R. Natoli, B. Searle, and B. T. Thole who introduced us to their multiple scattering and multiplet codes, and we are greatly endebted to them for numerous enlightening discussions and constant encouragements. One of us (C.B.) would like to thank Prs. J. C. Fuggle and G. A. Sawatzky for their kind hospitality in their laboratory. This work has been supported partially by EEC Contract ERBCHXCT930360.

JA941517B

(60) Xiao-Yu, K.; Morgenstern-Badarau, I. *Phys. Rev. B* **1992**, *46*, 3132.
(61) Xiao-Yu, K.; Morgenstern-Badarau, I.; Malfant, I. *Phys. Rev. B* **1993**, *47*, 5455.
(62) Kahn, O.; Pei, Y.; Verdaguer, M.; Renard, J. P.; Sletten, J. *J. Am. Chem. Soc.* **1988**, *110*, 782.
(63) Miller, J. S.; Epstein, A. J.; Reiff, W. M. *Acc. Chem. Res.* **1988**, *21*, 114.
(64) Manriquez, J. M.; Yee, G. T.; McLean, R. S.; Epstein, A. J.; Miller, J. S. *Science* **1991**, *252*, 1415.
(65) Stumpf, H. O.; Ouahab, L.; Pei, Y.; Grandjean, D.; Kahn, O. *Science* **1993**, *261*, 447.
(66) Galan-Mascaros, J. R.; Gomez-Garcia, C. J.; Borras-Almenar, J. J.; Coronado, E. *Adv. Mater.* **1994**, *6*, 221.
(67) Arrio, M.-A.; Sainctavit, P.; Cartier, C.; Brouder, C.; de Groot, F.; Verdaguer, M.; Mallah, T., unpublished.
(68) Karlin, K. D. *Science* **1993**, *261*, 701.
(69) George, S. J.; Lowery, M. D.; Solomon, E. I.; Cramer, S. P. *J. Am. Chem. Soc.* **1993**, *115*, 2968.
(70) Burgess, B. K. *Chem. Rev.* **1990**, *90*, 1377.
(71) Shadle, S. E.; Penner-Hahn, J. E.; Schugar, H. J.; Hedman, B.; Hodgson, K. O.; Solomon, E. I. *J. Am. Chem. Soc.* **1993**, *115*, 767.
(72) Solomon, E. I.; Jones, P. M.; May, J. A. *Chem. Rev.* **1993**, *93*, 2623.
(73) Westre, T. E.; Di Cicco, A.; Filipponi, A.; Natoli, C. R.; Hedman, B.; Solomon, E. I.; Hodgson, K. O. *J. Am. Chem. Soc.* **1994**, *116*, 6757.